FUDMA Journal of Sciences (FJS)
ISSN online: 2616-1370
ISSN print: 2645 - 2944
Vol. 10 No. 1, January, 2026, pp 166 – 174
DOI: https://doi.org/10.33003/fjs-2026-1001-4539

INFLUENCE OF MAGNETIC FIELD AND NANOPARTICLE TRANSPORT ON BOUNDARY LAYER FLOW: A NUMERICAL INVESTIGATION

Adekoya, Odunayo M., Akinfenwa, Olusheye A. and Fenuga, Olugbenga J.

Department of Mathematics, University of Lagos, Lagos State, Nigeria.

*Corresponding authors' email: adekoyaodunayo2@gmail.com

ABSTRACT

A study of magnetic field and nanoparticle transport on boundary layer flow of magnetohydrodynamic (MHD) nanofluid over a stretching vertical surface has been analyses numerically. By introducing appropriate similarity variables, the governing partial differential equations describing momentum, energy and concentration were reduced to nonlinear coupled Ordinary Differential Equations (ODE). Utilizing the shooting technique along exponentially fitted Simpson type block method is used to solve the Boundary value problems using computational software MAPLE 16. Numerical results for velocity, temperature and concentration profiles are presented and the effect of key parameters including magnetic field strength, Brownian motion, thermophoresis, internal heat generation and thermal radiation was analyzed. The computed Nusselt number and Sherwood number demonstrate excellent agreement with existing literature, confirming the stability and accuracy of the method used. The results reveal that magnetic effects reduce fluid velocity while thickening thermal and concentration boundary layers, whereas buoyancy forces, radiation and internal heat generation enhance momentum and heat transport. Nanoparticle diffusion is significantly influenced by thermophoresis and Brownian motion effects.

Keywords: Magnetohydrodynamics, Nanofluid, Heat and Mass Transfer, Exponentially Fitted Block Method, Thermal Radiation, Nanoparticle Transport

INTRODUCTION

Heat and mass transfer are of considerable interest because they occur in many geothermal, geophysical, technological and engineering processes such as nuclear reactors (Omokhuale and Uwanta, 2016), which can be successfully modelled by partial differential equations (PDEs) before being transformed into coupled nonlinear ordinary differential equations (ODEs) through similarity variables or the method of lines and then solved analytically or numerically. These processes are guided by fundamental principles and described by key governing equations including the continuity, momentum, energy and concentration equations. Heat transfer science deals with the rate of thermal energy transfer (Çengel and Ghajar, 2015) and has applications ranging from biological systems to household uses, building design, industrial processes, electronic devices and food processing. Heat is the form of energy transferred between systems due to temperature differences whereas mass transfer describes the transport of a chemical species from regions of higher concentration to regions of lower concentration.

Magnetohydrodynamics (MHD) involves the behavior of electrically conducting fluids in the presence of magnetic and electric fields (Davidson, 2017). In magnetohydrodynamic (MHD) flows, the application of a magnetic field plays a crucial role in heat and mass transfer processes. By modifying the motion of electrically conducting fluids, the magnetic field directly affects the transport of thermal energy and species concentration. This interplay is critical in various applications, notably in renewable energy systems, as well as in biomedical engineering for example, in controlling blood flow and facilitating targeted drug delivery (Rashid, 2018). Due to the significant effects of magnetic fields on boundary layers, MHD flow heat transfer has been widely studied.

Nanofluids, first proposed by Choi in 1995, are suspensions of nanoparticles in base fluids designed to enhance heat transfer performance (Choi, 1995). Nanofluids, which are engineered colloidal suspensions of nanoparticles in base fluids, have been shown to enhance heat and mass transfer performance. This enhancement arises primarily from the increased thermal conductivity and diffusivity provided by the nanoparticles, enabling more efficient heat exchange and faster diffusion of substances. The behavior of nanofluid heat and mass transfer depends on several factors, including nanoparticle type, concentration and size, as well as environmental conditions such as temperature, pressure and the presence of a magnetic field (Khan *et al.*, 2023). Investigating the parameters that influence heat and mass transfer in MHD nanofluid flows is crucial for optimizing industrial and technological applications. Key parameters such as the Prandtl number, chemical reaction rates and nanoparticle properties effects have a significant impact on flow dynamics, heat transfer rates and mass transfer characteristics. Sadighi *et al.* (2023) conducted a comparative study of temperature distributions under two different boundary conditions and the same approach was extended to the concentration profiles. They further investigated the effects of the Hartmann number, suction/injection parameter, and nanoparticle volume fraction on the local skin-friction coefficient using the Box–Behnken design. Usman and Sulaiman (2023) examined how Casson nanofluid flows across a semi-infinite flat plate imbedded in a porous media while being affected by heat radiation, Soret and pressure terms. Abbas (2025) investigated the heat and mass transfer characteristics of a chemically reactive hybrid nanofluid flow over an exponentially stretching sheet. This study placed particular emphasis on the influence of slip conditions and Lorentz forces on the boundary layer, concluding that hybrid nanoparticles significantly enhance thermal performance compared to mono-nanofluids, even in the presence of strong magnetic opposition. Uddin *et al.* (2017) examined magnetohydrodynamic nanofluid flow over a radiative surface, with particular emphasis on natural convection heat transfer along a horizontal plate, a topic for which physically realistic and practically relevant results remain scarce. Their work analysed the combined influence of velocity slip and zero mass flux boundary conditions on the boundary layer

flow over an upward-facing, nonlinearly radiating horizontal stretching sheet. Arshad *et al.* (2024) explored the mixed convective flow of hybrid nanofluids (Ag-MgO/Water) over a stretching surface, specifically focusing on the combined effects of Joule heating and a non-uniform heat source. Their findings revealed that temperature dependent viscosity and slip conditions play a decisive role in determining the thickness of the thermal boundary layer, which is essential for optimizing electronic cooling systems.

Khan *et al.* (2023) addressed an existing research gap by analysing the impact of slip boundary conditions on velocity, temperature and concentration fields in nanofluid boundary layer flow, while also accounting for viscous dissipation effects. Pavithra *et al.* (2025) conducted a statistical and numerical investigation into how nanoparticle shape factors (spherical, cylindrical and platelet) influence heat transfer in MHD nanofluid flow over a stretching sheet. Their study incorporated an exponential heat source/sink and a first order chemical reaction, demonstrating that the geometric configuration of nanoparticles is a primary determinant of the local Nusselt and Sherwood numbers. Kho *et al.* (2018) explored the combined influence of thermal radiation and magnetic fields on the velocity, temperature and concentration profiles of a Casson nanofluid flowing over a stretching sheet with constant wall temperature. Kumar *et al.* (2025) examined the magnetohydrodynamic (MHD) flow of a non-Newtonian Casson nanofluid over a porous surface for solar energy applications. Their work analysed the interplay between Cattaneo-Christov heat flux and thermal radiation, providing new insights into how high temperature environments affect the entropy generation and thermal stability of the boundary layer in solar collectors.

Inspired by the work of Noghrehabadi, Pourrajab and Ghalambaz (2012), their investigation which focus on the effect of slip factor, Prandtl number, lewis parameter, Brownian motion and thermophersis parameter on the heat transfer characteristic of stretching sheet, this study will be extending their work by introducing other critical parameters previously unaddressed: magnetic field effects, local thermal and solutal Grashof numbers, thermal radiation, and internal heat generation. This expansion facilitates a more comprehensive investigation into the Magnetohydrodynamic (MHD) nanofluid flow over a stretching sheet. To analyse the system, the governing partial differential equations (PDEs) representing the boundary layer problem are reduced to a system of nonlinear ordinary differential equations (ODEs) using appropriate similarity transformations. The resulting ODEs are solved using an exponentially fitted Simpson's type block method integrated with a shooting technique. While block methods have demonstrated notable efficiency and stability in solving single-fluid flow and boundary value problems (Olabode *et al.,* 2024; Kwari *et al.,* 2021), and a few studies such as those of Oyelakin *et al.* (2020), Phang and Abdulmajid (2015) have extended their application to MHD and nanofluid flow problems. The exponentially fitted block method adopted in this study follows the approach of Faniyi *et al.* (2023), incorporating exponential fitting to improve accuracy in solving differential equations arising in MHD nanofluid heat and mass transfer. This combination provides a stable and computationally efficient alternative to conventional numerical techniques.

MATERIALS AND METHODS

Governing Equation

Consider a steady, two dimensional, incompressible, viscous flow of a nanofluid over a stretching surface. The surface velocity varies linearly and it expresses as $U_w(x)=cx$, where c is a constant and x is the coordinate along the stretching surface. The nanofluid flow occurs at $y=0$, with y being the coordinate perpendicular to the stretching surface. The wall temperature T_w and the nanoparticle volume fraction φ_w are constant at the stretching surface. As $y\to\infty$, the temperature T and the nanoparticle φ volume fraction approaches the constant ambient values T_N and φ_N repectively. (Extended from Noghrehabadi *et al.* 2012)

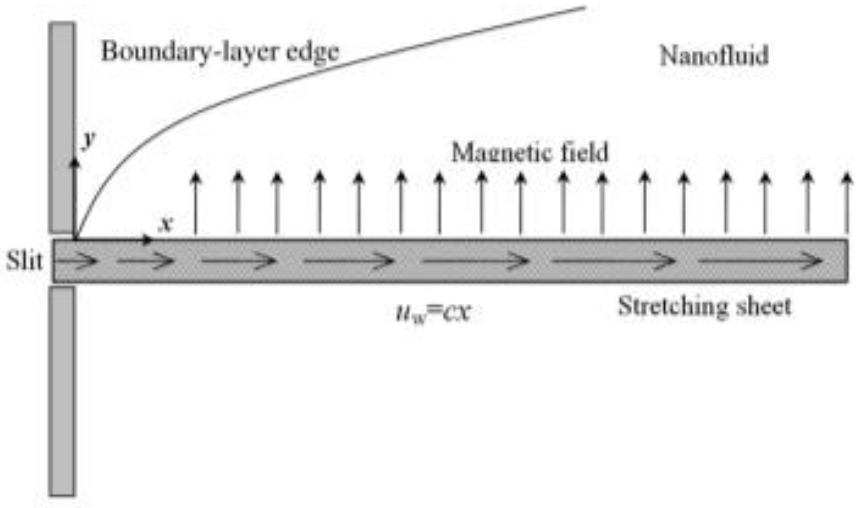

Figure 1: Boundary Layer Configuration

Continuity Equation

$$\frac{\partial u}{\partial x}+\frac{\partial v}{\partial y}=0 \quad (1)$$

Momentum Equation

$$u\frac{\partial u}{\partial x}+v\frac{\partial u}{\partial y}=\upsilon\left(\frac{\partial^2 u}{\partial x^2}+\frac{\partial^2 u}{\partial y^2}\right)-\sigma\frac{\beta_o^2 u}{\rho}+g\beta_t\left(T-T_\infty\right)+g\beta_c\left(\varphi-\varphi_\infty\right) \quad (2)$$

Energy Equation

$$u\frac{\partial T}{\partial x}+v\frac{\partial T}{\partial y}=\alpha\left(\frac{\partial^2 T}{\partial x^2}+\frac{\partial^2 T}{\partial y^2}\right)+\tau\left\{D_B\left(\frac{\partial\varphi}{\partial x}\frac{\partial T}{\partial x}+\frac{\partial\varphi}{\partial y}\frac{\partial T}{\partial y}\right)+\frac{D_T}{T_\infty}\times\left[\left(\frac{\partial T}{\partial x}\right)^2+\left(\frac{\partial T}{\partial y}\right)^2\right]\right\}+\frac{Q_\infty}{\rho C_p}\left(T-T_\infty\right)-\frac{1}{\rho C_p}\frac{\partial q_r}{\partial y} \quad (3)$$

Concentration Equation

$$u\frac{\partial\varphi}{\partial x}+v\frac{\partial\varphi}{\partial y}=D_B\left(\frac{\partial^2\varphi}{\partial x^2}+\frac{\partial^2\varphi}{\partial y^2}\right)+\frac{D_T}{T_\infty}\left(\frac{\partial^2 T}{\partial x^2}+\frac{\partial^2 T}{\partial y^2}\right) \quad (4)$$

The boundary condition for the velocity components with partial slip condition at the wall $(i.e\ y=0)$ for nanoparticle fraction and temperature are defined as

$$v=0, u=U_w(x)-U_s, T=T_w,\ \varphi=\varphi_w \quad at\ y=0 \quad (5)$$

$$v=u=0, T=T_w, \varphi=\varphi_w \quad at\ y=\infty \quad (6)$$

Where *u and v* are the velocity components along the axis *x* and *y* respectively, *p* is the fluid pressure, α is the thermal diffusivity, υ is the kinematic velocity, ρ_f is the density of the base fluid, ρ_p is the density of the particle, D_B is the Brownian diffusion coefficient, D_T is the thermophoresis diffusion coefficient, ρ being the density, C_p the specific heat at constant pressure, B_0 is the magnetics strength, B_T is the thermal expansion coefficient, σ is the electrical conductivity, *g* is the acceleration due to gravity, *Q* is the internal heat generation.

The radiative heat flux q_r is described by Roseland approximation such that

$$q_r=-\frac{4\sigma^*}{3\delta}\frac{\partial T^4}{\partial y} \quad (7)$$

Where σ^* and δ are the Stefan-Boltzmann constant and the mean absorption coefficient respectively. We assume that the temperature difference within the flow is sufficiently small so that the T^4 can be expressed as a linear function after using Taylor series to expand T^4 about the free stream temperature T_∞ and neglecting higher order terms. This result is the following approximation:

$$T^4\cong 4T_\infty^3 T-3T_\infty^4 \quad (8)$$

Using (7) and (8) in (3), we obtain

$$\frac{\partial q_r}{\partial y}=-\frac{16\sigma^* T_\infty^3}{3\delta}\frac{\partial T^2}{\partial y} \quad (9)$$

We introduce a stream function ψ defined with by

$$u=\frac{\partial\psi}{\partial y},\quad v=-\frac{\partial\psi}{\partial x} \quad (10)$$

so that the continuity equation is satisfied identically.

we also introduce the dimensionless variable in equation (11a) and (11b)

$$\psi=(c\nu)^{1/2}xf(\eta),\qquad \eta=(c/\nu)^{1/2}y \quad (11a)$$

$$\theta(\eta)=\frac{T-T_\infty}{T_w-T_\infty},\qquad \beta(\eta)=\frac{\varphi-\varphi_\infty}{\varphi_w-\varphi_\infty} \quad (11b)$$

Then substituting in equations (1) - (4), we obtain the following ordinary differential equations

$$f'''(\eta)+f(\eta)f''(\eta)-f'^2(\eta)-M_x f'(\eta)+Gr_x\theta(\eta)+Gc_x\beta(\eta)=0 \quad (12)$$

$$\left(\frac{1}{pr}+Ra\right)\theta''(\eta)+Nb\beta'(\eta)\theta'(\eta)+Nt\theta'^2(\eta)+f(\eta)\theta'(\eta)+Q\theta(\eta)=0 \quad (13)$$

$$\beta''(\eta)+\frac{Nt}{Nb}\theta''(\eta)+Lef(\eta)\beta'(\eta)=0 \quad (14)$$

The parameters of Gr_x, Gc_x, M_x, Pr, Nb, Nt, Le, Q, and λ are defined by

$$\left.\begin{aligned} &Gr_x=\frac{g\beta_t}{C^2 x}\left(T_w-T_\infty\right),\ M_x=\frac{\sigma\beta_o^2}{\rho C},\ \ Pr=\frac{\nu}{\alpha},\ \ Le=\frac{\nu}{D_\beta},\\ &Nb=\frac{D_\beta\tau}{\nu}\left(\varphi_w-\varphi_\infty\right),\ Nt=\frac{D_T\tau}{T_\infty\nu}\left(T_w-T_\infty\right),\ Ra=\frac{16\sigma^* T_\infty^3}{\nu\rho Cp3\delta\alpha}\\ &\lambda=N\rho(c\nu)^{1/2},\ Q=\frac{Q_\infty}{C\rho c_p},\ \ Gc_x=\frac{g\beta_c}{C^2 x}\left(\varphi_w-\varphi_\infty\right)\end{aligned}\right\} \quad (15)$$

Here Gc_x, M_x, Pr, Le, Nb, Nt, R, λ, Q and Gr_x, denote Local solutal grashof number, Magnetic parameter, Prandtl number, Lewis number, the Brownian motion parameter, Thermophoresis parameter, Radiation parameter, slip factor, Internal heat generation, and Local thermal grashof number parameter respectively.

equations (12) – (14) are solved under to the following condition

$$\text{At } \eta=0: \quad f=0,\quad f'=1,\quad \theta=1,\quad \beta=1 \quad (16)$$

$$\text{At } \eta\to\infty: \quad f'=0,\quad \theta=0,\quad \beta=0 \quad (17)$$

Where prime denote differentiation with respect to η.

Method of Solution

The coupled nonlinear ODEs governing the momentum, energy and concentration fields given by equations (12-14) together with the boundary conditions (16–17), constitute a boundary value problem. Due to the strong nonlinearity and coupling of the system, closed-form solution is not feasible therefore a numerical approach is employed.

To facilitate numerical integration, the higher order differential equations are first transformed into an equivalent system of first order ODEs. The following substitutions are introduced

$$f=y_1,\ f'=y_2,\ f''=y_3,\ \theta=y_4,\ \theta'=y_5,\ \beta=y_6,\ \beta'=y_7$$

Using these definitions, equation (12-14) are rewritten as a system of seven first order equations

$$\begin{aligned} y_1' &= y_2\\ y_2' &= y_3\\ y_3' &= -y_1y_3+y_2^2-M_x y_2-Gry_4-Gcy_6\\ y_4' &= y_5\\ y_5' &= \frac{\left(-Nby_7y_5-Nty_5^2-y_1y_5-Qy_4\right)}{\left(\frac{1}{Pr}+R\right)}\\ y_6' &= y_7\\ y_7' &= -\frac{Nt}{Nb}y_4-Ley_1y_7 \end{aligned} \quad (18)$$

subject to the transformed boundary conditions at $\eta=0$ and $\eta\to\infty$.

The boundary conditions prescribed at infinity are numerically handled by truncating the semi-infinite domain $(0,\infty)$ to a finite computational domain $(0,\eta_{max})$ after several numerical experiments. It was observed that $\eta_{max}=15$ is sufficient to ensure that the asymptotic boundary condition $f'(\eta_{max})\simeq 0,\ \theta(\eta_{max})\simeq 0,\ \beta(\eta_{max})\simeq 0$ are satisfied with acceptable accuracy, increasing η_{max} beyond this value produced no significant change in the numerical results. At $\eta=0$ the boundary conditions specify $f(0)=0$, $f'(0)=1$, $\theta(0)=1$, $\beta(0)=1$ while the unknown initial condition $f''(0)=r_1$, $\theta'(0)=r_2$, $\beta'(0)=r_3$ must be determined such that the far fluid boundary conditions are satisfied. These unknown initial values are treated as shoot parameters. An initial guess for (r_1, r_2, r_3) is chosen and the resulting initial value problem is intergtared numerically with exponentially

fitted Simpson's type block method. The guesses are iteratively refined until the boundary conditions at $\eta=\eta_{max}$ are satisfied. The unknown initial slopes are iteratively updated using a newton type correction scheme within the shooting technique until the far field boundary condition are satisfied with a tolerance of 10^{-6}.

The exponentially fitted block method which will be used in this study to solve the IVPs emanated from boundary layer problem of MHD nanofluid flow is the algorithm developed by Faniyi *et al.* (2023). The block method has the expression

$$u(x)=\alpha_0 y_n+\sum_{i=0}^{3} B(\omega,\mathrm{h})\, f_{n+i}, \qquad (19)$$

where $\alpha_0=1$, B is a function depending on ω and h. (19) is evaluated at point x_{n+i}, $i=0(1)3$, the 3 step exponentially fitted backward difference method were obtained as followed.

$$y_{n+1}=y_n+\xi_1((12-16e^{2hw}\mathrm{h}w+5e^{3hw}\mathrm{h}w+e^{hw}(-12+23\mathrm{h}w))f_n+(-36+36e^{hw}-23\mathrm{h}w-21e^{2hw}\mathrm{h}w+8e^{3hw}\mathrm{h}w)f_{n+1}-$$
$$\left(e^{3hw}\mathrm{h}w+e^{hw}(36-21\mathrm{h}w)-4(9+4\mathrm{h}w)\right)f_{n+2}+\left(-12-5\mathrm{h}w+e^{2hw}\mathrm{h}w+e^{hw}(12-8\mathrm{h}w)\right)f_{n+3})$$
$$y_{n+2}=y_n+\xi_2((3+7e^{hw}\mathrm{h}w+e^{3hw}\mathrm{h}w-e^{2hw}(3+2\mathrm{h}w))f_n+(-9-7\mathrm{h}w+4e^{3hw}\mathrm{h}w+e^{2hw}(9-15\mathrm{h}w))f_{n+1}+$$
$$(9-9e^{2hw}+2\mathrm{h}w+15e^{hw}\mathrm{h}w+e^{3hw}\mathrm{h}w)f_{n+2}+(-3+3e^{2hw}\mathrm{h}w-\mathrm{h}w-4e^{hw}\mathrm{h}w-e^{2hw}\mathrm{h}w)f_{n+3})y_{n+3}=y_n+\xi_1(9(-4+4e^{3hw}-3\mathrm{h}w)f_n-$$
$$(9e^{2hw}\mathrm{h}w)f_{n+1}+(9(4+9e^{hw}\mathrm{h}w+e^{3hw}(-4+3\mathrm{h}w)))f_{n+2}+3(-4+4e^{3hw}-3\mathrm{h}w-9e^{2hw}\mathrm{h}w)f_{n+3}) \qquad (20)$$

Where $\xi_1=\frac{1}{12w(e^{hw}+1)^3}$, $\xi_2=\frac{1}{3w(e^{hw}+1)^3w}$,

The order of accuracy is uniformly 5, while error constant is

$$C_{p+1}=\begin{pmatrix} -\frac{95}{288}\left(wy^{(5)}(x)-y^{(6)}(x)\right)\mathrm{h}^6+O(\mathrm{h})^7 \\ -\frac{14}{45}\left(wy^{(5)}(x)-y^{(6)}(x)\right)\mathrm{h}^6+O(\mathrm{h})^7 \\ -\frac{51}{160}\left(wy^{(5)}(x)-y^{(6)}(x)\right)\mathrm{h}^6+O(\mathrm{h})^7 \end{pmatrix}.$$

RESULTS AND DISCUSSION

This section presents the performance of the numerical method. The transformed system of nonlinear ODEs was solved using the exponentially fitted block method combined with shooting techniques. Table 1 compares the present Nusselt and Sherwood numbers with the results of Khan & Pop (2010) and Noghrehabadi *et al.* (2012). The close agreement across all parameter values confirms the accuracy and reliability of the method. Table 2 reports the computed skin friction coefficient $f''(0)$, local Nusselt number $\theta'(0)$ and nanoparticle Sherwood number $\beta'(0)$for variations in *M*, *Gr*, *Gc*, *Q* and *Ra.* Magnetic field strength, buoyancy effects, heat generation and radiation significantly influence the flow, heat and mass transfer characteristics.

Table 1: Comparison of Results for Nusselt Number and Sherwood Number when Le = 10, Pr= 10

Nt	Nb	Nur			Shr		
		Khan&pop (2010)	Noghr *et al.* (2012)	Present work	Khan&pop (2010)	Noghr *et al.* (2012)	Present work
0.1	0.1	0.9524	0.95237	0.95267	2.1294	2.12939	2.12910
0.2	0.1	0.6932	0.69317	0.69319	2.2740	2.27402	2.27397
0.3	0.1	0.5201	0.52007	0.52009	2.5286	2.52863	2.52862
0.4	0.1	0.4026	0.40258	0.40259	2.7952	2.79517	2.79516
0.5	0.1	0.3211	0.32105	0.32107	3.0351	3.03514	3.03513
0.1	0.2	0.5056	0.50558	0.50559	2.3819	2.38187	2.38186
0.1	0.3	0.2523	0.25215	0.25216	2.4100	2.41001	2.41001
0.1	0.4	0.1194	0.11940	0.11941	2.3997	2.39965	2.39965
0.1	0.5	0.0543	0.05425	0.54255	2.3836	2.38356	2.38356

Table 2: Computation Showing $f''(0)$, $\theta'(0)$ and $\beta'(0)$ when *Le*=10, *Pr*=10, λ=0,*Nb*=0.1, *Nt*=0.1

M	*Gr*	*Gc*	Q	Ra	$-f''(0)$	$-\theta'(0)$	$-\beta'(0)$
0.1	0.1	0.1	0.1	2	0.94207304	0.25287855	2.2736442
1.0					1.32257449	0.15998972	2.2090314
5.0					2.38603963	0.14508583	2.1124425
	0.5				0.67752426	0.31926572	2.3253451
	1.5				0.13004549	0.38806914	2.4212796
		0.5			0.85007256	0.26055287	2.2858774
		1.5			0.62477557	0.27739364	2.3150508
			0.2		0.93135707	0.13244648	2.3248931
			0.3		0.91237065	0.07347108	2.4044945
				3	0.93219750	0.19012320	2.2934515
				7	0.91671746	0.11219096	2.3175684

Effects of Variation of Parameters on the Velocity Profiles

Fig. 2 -6 shows the influence of parameters on the velocity profile, in fig. 2 (*Nb*), It was observed that the velocity profile escalates with a rise in values. This is because the intensified random motion of nanoparticles enhances the kinetic energy and thermal state of the fluid. In convective flows, this temperature rise increases the thermal buoyancy force, which in turn accelerates the fluid flow. An increase in thermophoresis *Nt* in fig. 3 values lead to an elevation in fluid velocity. The thermophoretic force moves particles from the

hot surface to the ambient cold fluid, thickening the thermal boundary layer. This enhancement in the thermal state strengthens the buoyancy effects, providing a slight push or acceleration to the fluid. In fig. 4, the velocity profiles corresponding to the magnetic parameter M show a consistent reduction in fluid motion as the magnetic intensity becomes stronger, cases associated with weaker magnetic influence exhibit higher velocities while those subjected to stronger magnetic fields experience noticeable damping. This behavior is attributed to the Lorentz force, which resists fluid motion in electrically conducting flows. For the internal heat generation parameter Q in fig. 5, velocity rises when internal heat production becomes more significant. Additional thermal energy promotes buoyancy, giving rise to an accelerated flow near the plate. With the radiation parameter Ra in fig. 6, velocity also increases as radiative effects grow stronger. Radiative heating elevates the temperature of the fluid, thereby strengthening buoyancy and enhancing the momentum boundary layer thickness.

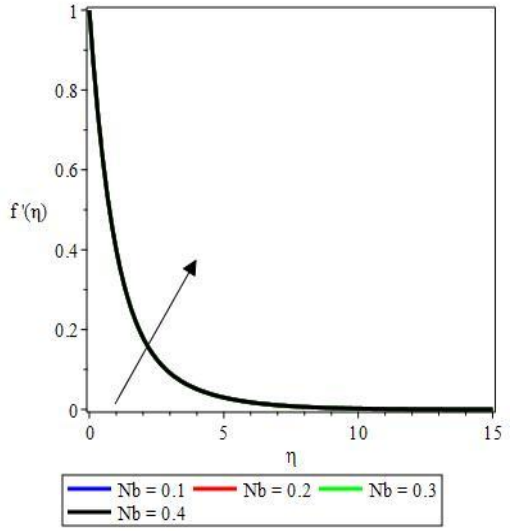

Figure 2: Effect of Nb on Velocity Profile when $Le = 10, Pr = 10, Nt = 0.1, Gc = 0.1, Q = 0.1, Gr = 0.1, M = 0.1, Ra = 2$

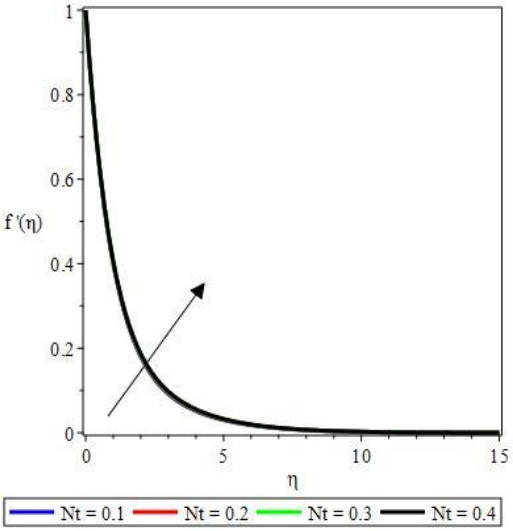

Figure 3: Effect of Nt on Velocity Profile when Le=10,Pr=10,Gr=0.1,,Nb=0.1,Q=0.1,Gc=0.1,M=0.1,Ra=2

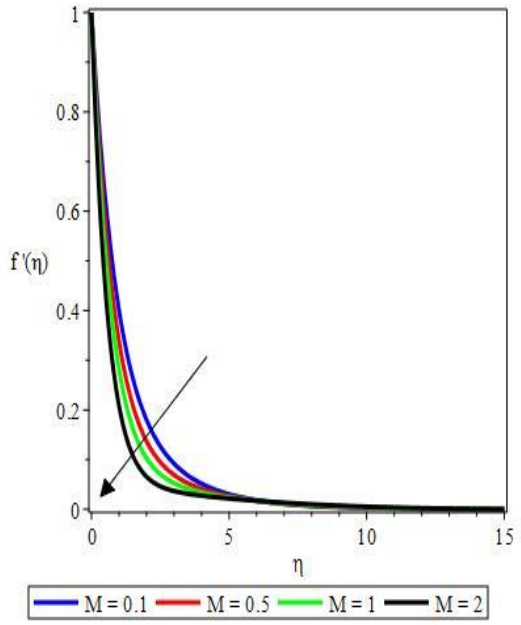

Figure 4: Effect of M on Velocity Profile when Le=10,Pr=10,Nt=0.1,Nb=0.1,Q=0.1,Gr=0.1,Gc=0.1,Ra=2

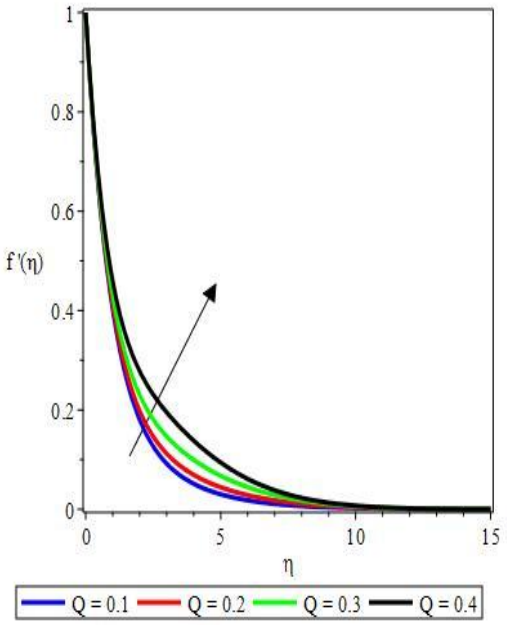

Figure 5: Effect of Q on Velocity Profile when Le=10,Pr=10,Nt=0.1,Nb=0.1,Gr=0.1,Gc=0.1,M=0.1,Ra=2

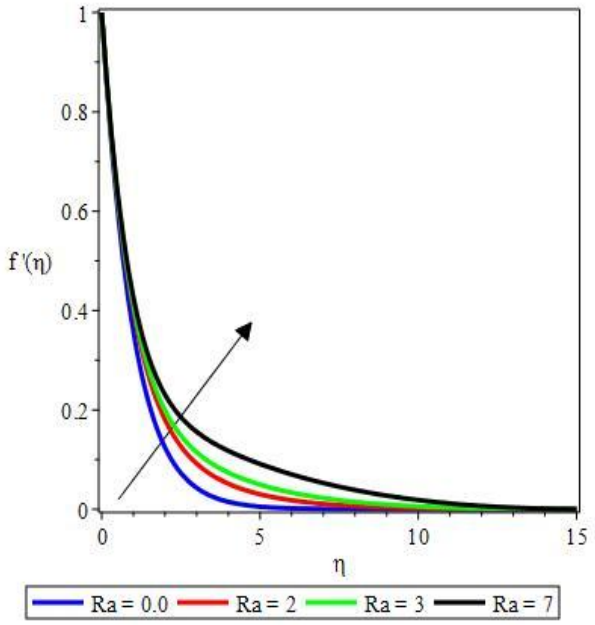

Figure. 6: Effect of Ra on Velocity Profile When Le=10,Pr=10,Nt=0.1,Nb=0.1,Q=0.1,Gr=0.1,Gc=0.1,M=0.1

Effects of Variation of Parameter on the Temperature Profile

Fig. 7 - 11 shows the effect of parameters on the temperature profile, for Brownian motion *Nb* in fig. 7, the temperature profile escalates as rises describes the random, erratic movement of nanoparticles within the base fluid. As this parameter increases, the collisions between particles and fluid molecules become more frequent and energetic. This process generates additional heat, consequently boosting the thickness of the thermal boundary layer. Increasing the values thermophoresis *Nt* in fig. 8, results in an elevation of the fluid temperature. Thermophoresis is the phenomenon where a temperature gradient exerts a force on particles, propelling them from the hot surface toward the cold region. This transport of hot particles into the cooler fluid layers effectively raises the overall temperature distribution. In fig. 9 which is magnetic parameter M, the temperature distributions indicate that stronger magnetic influence produces a thicker thermal boundary layer. Magnetic damping releases additional heat into the fluid, raising its temperature throughout the boundary layer. The internal heat generation Q parameter in fig. 10 has a direct heating effect. Stronger internal heat production leads to a marked rise in the temperature distribution and thickens the thermal boundary layer. Radiation *Ra* in fig. 11 also plays a significant role in increasing the fluid temperature. Stronger radiative influence contributes additional thermal energy, causing the temperature to rise throughout the boundary layer and enlarging the thermal layer thickness.

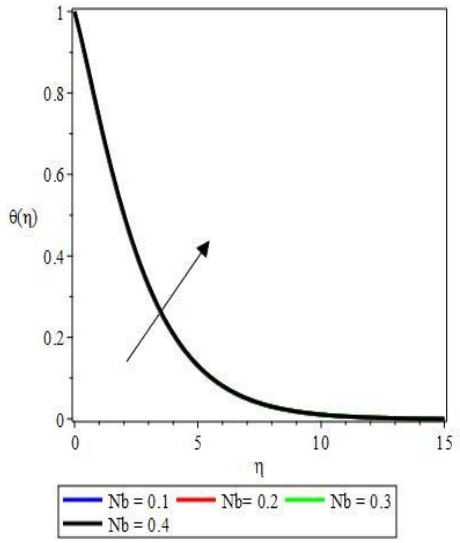

Figure 7: Effect of Nb on Temperature Profile when Le=10,Pr=10,Nt=0.1,Gc=0.1,Q=0.1,Gr=0.1,M=0.1,Ra=2

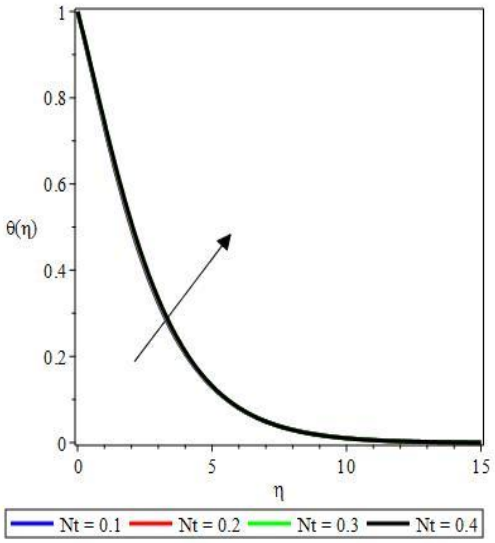

Figure 8: Effect of Nt on Temperature Profile when Le=10,Pr=10,Gr=0.1,Nb=0.1,Q=0.1,Gc=0.1,M=0.1,Ra=2

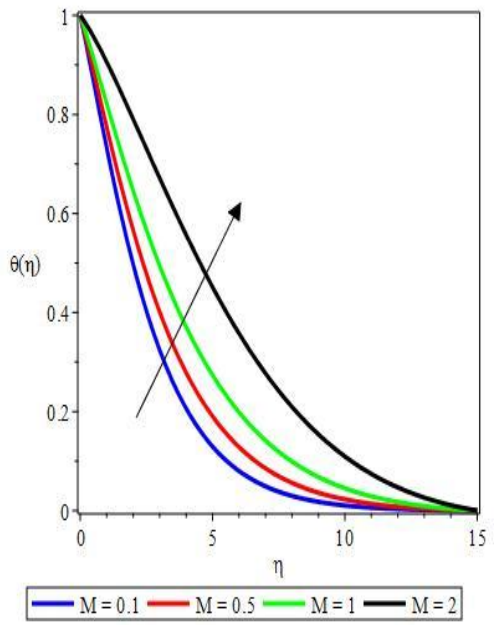

Figure 9: Effect of M on Temperature Profile when Le=10,Pr=10,Nt=0.1,Nb=0.1,Q=0.1,Gr=0.1,Gc=0.1,Ra=2

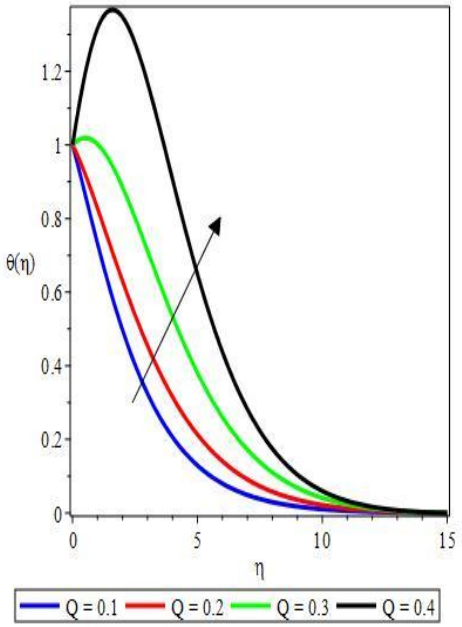

Figure 10: Effect of Q on Temperature Profile when Le=10,Pr=10,Nt=0.1,Nb=0.1,Gr=0.1,Gc=0.1,M=0.1,Ra=2

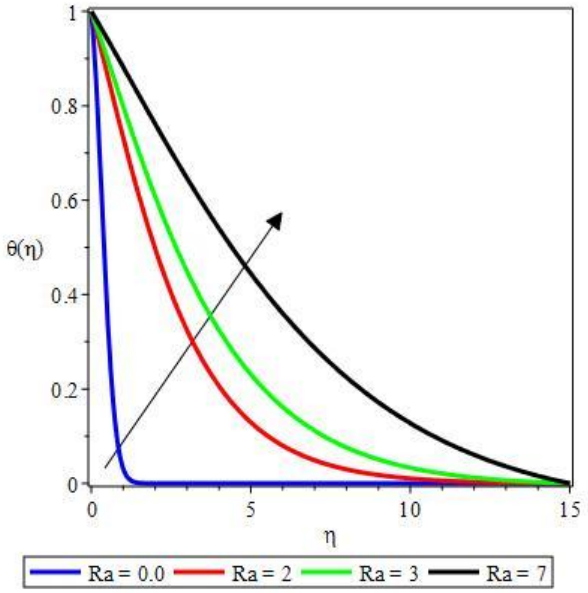

Figure 11: Effect of Ra on Temperature Profile when Le=10,Pr=10,Nt=0.1,Nb=0.1,Q=0.1,Gr=0.1,Gc=0.1,M=0.1

Effects of Variation of Parameters on Concentration Profile

Fig. 12 - 16 shows the effect of parameters on the concentration profile, fig. 12 shows the Brownian Motion *Nb* effect, the concentration profile decreases with an increase in values. While Brownian motion heats the fluid, it simultaneously acts as a powerful dispersing mechanism. Higher random motion helps spread the nanoparticles more uniformly throughout the fluid and away from the boundary, thereby reducing the nanoparticle concentration near the wall. Conversely, an increase in thermophoresis *Nt* in fig. 13 elevates the nanoparticle concentration. Since the thermophoretic force tends to propel nanoparticles from the hot surface toward the colder ambient fluid, it leads to a build-up of particles within the boundary layer. As a result, both the thermal and solutal (concentration) boundary layer thicknesses are elevated in the boundary layer regime. The concentration profiles reveal that stronger magnetic effects *M* in fig. 14 cause a buildup of nanoparticles near the plate. The magnetic resistance slows the flow, reducing convective transport and allowing more particles to remain close to the boundary, resulting in a thicker concentration layer. In fig. 15 the internal heat generation *Q* parameter contributes to thermal gradients that encourage thermophoretic movement of nanoparticles away from the heated surface. As a consequence, stronger heat generation reduces nanoparticle concentration near the wall. Radiation *Ra* in fig. 16 has a similar influence. Enhanced radiative heating strengthens thermophoretic forces, driving nanoparticles away from the plate and producing a thinner concentration boundary layer.

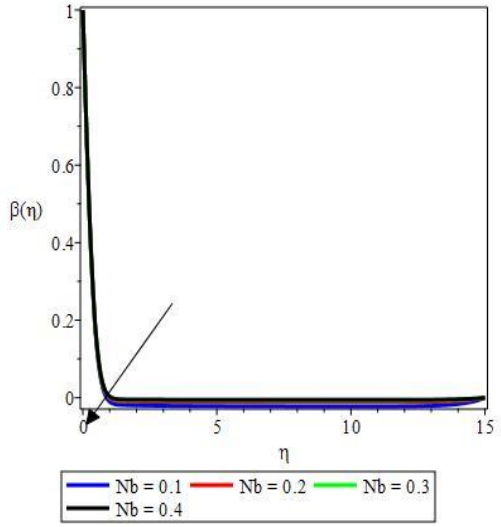

Figure 12: Effect of Nb on Concentration Profile when Le=10,Pr=10,Nt=0.1,Q=0.1,Gc=0.1,Gr=0.1,M=0.1,Ra=2

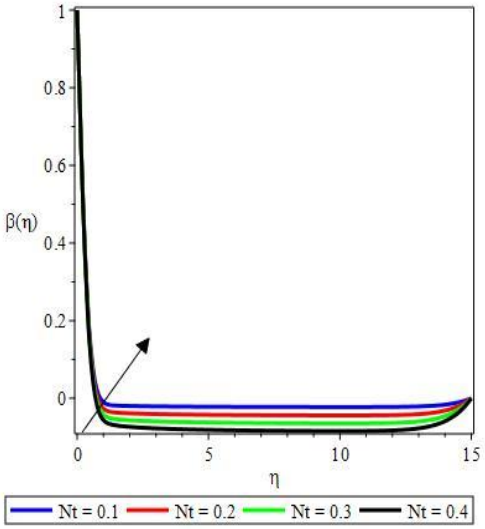

Figure 13: Effect of Nt on Concentration Profile when Le=10,Pr=10,Gr=0.1,Nb=0.1,Q=0.1,Gc=0.1,M=0.1,Ra=2

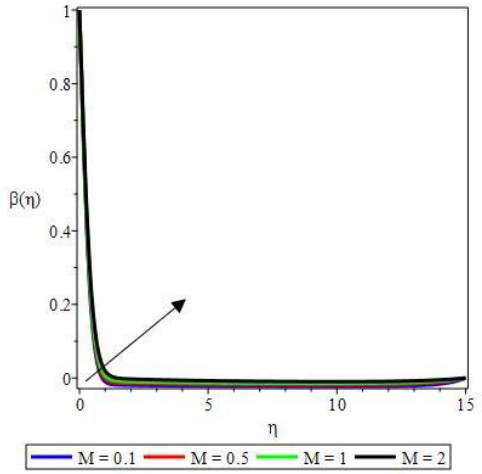

Figure 14: Effect of M on Concentration Profile when Le=10,Pr=10,Nt=0.1,Nb=0.1,Q=0.1,Gr=0.1,Gc=0.1,Ra=2

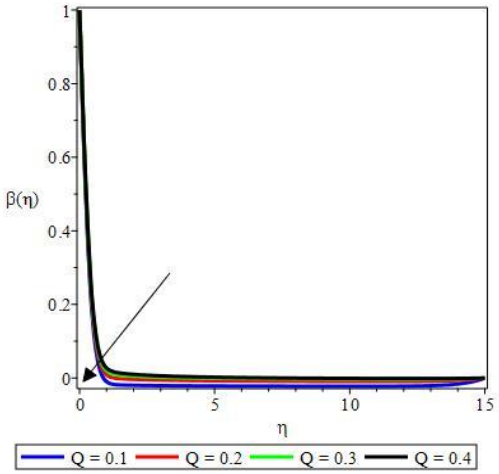

Figure 15: Effect of Q on Concentration Profile when Le=10,Pr=10,Nt=0.1,Nb=0.1,Gr=0.1,Gc=0.1,M=0.1,Ra=2

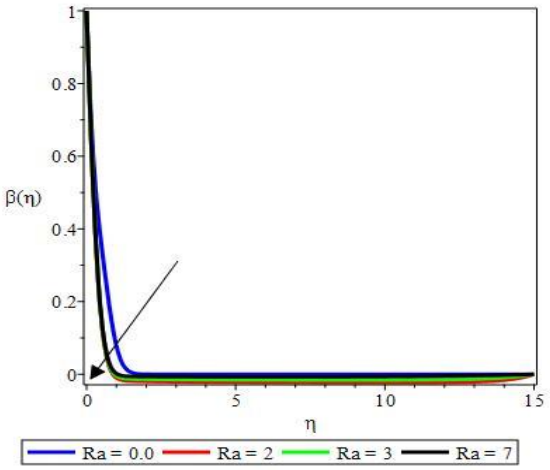

Figure 16: Effect of Ra on Concentration Profile when Le=10,Pr=10,Nt=0.1,Nb=0.1,Q=0.1,Gr=0.1,Gc=0.1,M=0.1

CONCLUSION

An exponentially fitted block method coupled with a shooting technique developed by Faniyi *et al.* (2023) was applied to the analysis of MHD nanofluid boundary layer flow over a stretching surface. The study extended the work of Nogrehabadi *et al.*, (2012) boundary layer models by including the effects of magnetic fields, buoyancy forces, thermal radiation and internal heat generation. Numerical results indicate that magnetic fields suppress fluid velocity and thicken thermal and nanoparticle concentration boundary layers, whereas buoyancy forces, radiation and heat generation enhance momentum, heat and mass transport. Nanoparticle distributions are strongly influenced by Brownian motion and thermophoresis effects. The method used provides a reliable tool for investigating complex coupled nonlinear interactions and offers valuable insights for engineering applications, including energy systems, coating processes and thermal management.

REFERENCES

Abbas, T. (2025). Slip effects and Lorentz force impacts on chemically reactive hybrid nanofluid over an exponentially stretching sheet. *International communications in heat and mass transfer, i60, 108214.* Doi.org/ https://doi.org/10.1016/j.icheatmasstransfer.2024.108214.

Arshad, M., Ahmed, A., & Hassan, A. (2024). Mixed convective hybrid nanofluid flow a stretching surface with joule heating and non-uniform heat source effects. *Journal of magnetism and magnetic material,* 592, 171805. Doi.org/ https://doi.org/10.1016/j.jmmm.204.171805.

Cengel, Y. A., & Ghajar, A. J. (2015). Heat and mass transfer: Fundamentals and applications (5th ed.). McGraw-Hill Education.

Choi, S.U.S., & Eastman, J. A. (1995). Enhancing thermal conductivity of fluids with Nanoparticles. *In D.A. Siginer & H.P. Wang (Eds), Developments and Applications of Non-Newtonian flow,* 231, 99-105.

Davidson, P. A. (2017). *Introduction to magnetohydrodynamics* (2nd ed.). Cambridge University Press.

Faniyi, O. E., Modebei M.I., & Olaiya, O.O. (2023). A three- step Simpson's type exponentially fitted backward difference method for the numerical solution of first order ordinary differential equations. *Journal of the Nigerian mathematical society.* 42(3), 273-285.

Khan, K., Javed, M., Ullah, M., & Riaz, M. (2023). Heat and mass transport analysis for Williamson MHD nanofluid flow over a stretched sheet. *Elsevier,* DOI: https://doi.org/10.1016/j.rinp.2023.106873.

Kho, Y., Hussanan, A., Sarif, N., & Ismail, Z. (2018). Thermal radiation effects on MHD with flow heat and mass transfer in casson nanofluid over a stretching sheet. *MATEC web of conference,* 150(2018), DOI: https://doi.org/10.1051/matecconf/201815006036.

Kumar, R. Sravani, J., & Rao, V.S. (2025). Entropy generation and thermal stability of MHD Casson nanofluid flow over a porous surface for solar energy applications. *Case studies in thermal engineering,* 65, 105421. Doi.org/ https://doi.org/10.1016/j.csite.2024.105421.

Kwari, A. I., Sirisena, U. N., & Thomas, R. (2021). A block method for the numerical solution of second-order boundary value problems in fluid flow. *Alexandria Engineering Journal*, 60(6), 5627–5637.

Noghrehabadi, A., Pourrajeb, R., & Mohammad, G. (2012). Effect of Partial Slip Boundary Condition on the Flow and Heat Transfer of Nanofluids Past Stretching Sheet Prescribed Constant Wall Temperature. *International Journal of Thermal Science,* 54(2012), 253-261.

Olabode, B.T., Momoh, A.L., & Senewo, E.O. (2024). Derivative block methods for fourth order boundary value problems of ordinary differential equations. *Proceedings of the Nigerian society of physical sciences conferences,* 1(2024), DOI: https://doi.org/10.61298/pnspsc.2024.1.80.

Omokhuale, E., & Uwanta, I.J. (2016). Viscoelastic Fluid follow with Heat and Mass Transfer in the Presence of Induced Magnetic filled. *International Journal of Science for Global Sustainability,* 2(3), 88-99.

Oyelakin, I., Adeyeye, O., Sibanda, P., & Omar, Z. (2020). On a New Block Method for an MHD Nanofluid flow with an Exponentially Decaying Internal Heat Generation. *International Journal Numerical Method Fluids.* 93(2021), 1816-1824.

Pavithra R. Venkatesh, P., & Reddy, G.J. (2025). Influence of nanoparticle shape factors on MHD nanofluid flow over a stretching sheet. A statistical and numerical approach. *Numerical heat transfer Part A: applications,* 87(2), 145-163.

Phang, P.S., & Abdulmajid, Z. (2015). Solving boundary layer problem using fifth order block method. *AIP conference proceedings,* DOI: https://doi.org/10.1063/1.4913012.

Rashidi, M. M., Yang, Z., Bhatti, M. M., & Abbas, M. A. (2018). Heat and mass transfer analysis on MHD blood flow of Casson fluid model due to peristaltic wave. *Thermal Science, 22*(6A), 2439–2448.

Sadighi, S., Afshar, H., Jabbari, M., & Ashtiani, H. (2023). Heat and mass transfer for MHD nanofluid flow on a porous stretching sheet with prescribing boundary conditions. *Cas studied in thermal Engineering Elsevier,*49(1), DOI: https://doi.org/10.1016/j.csite.2023.103345.

Uddin, M., Sohail, A., Beg, O., & Ismail, A. (2017), Numerical solution of MHD slip flow of a nanofluid past a radiating plate with Newtonian heating. A lie group approach. *Alexandria Engineering journal Elsevier,* 57(2018), 2455-2464.

Usman, S. & Sulaiman, S. (2023). Heat and Mass transfer analysis for the MHD flow of Casson nanofluid in the presence of thermal radiation. *FUDMA journal of science,* 7(2), 188-198.